Thermochimica Acta 520 (2011) 25–32

Contents lists available at ScienceDirect

Thermochimica Acta

journal homepage: www.elsevier.com/locate/tca

Thermal conductivity and interfacial energies of solid Sn_3Sb_2 in the Sn–Sb peritectic system

Y. Kaygısız[a], Y. Ocak[a,b], S. Aksöz[c], K. Keşlioğlu[b], N. Maraşlı[b,*]

[a] Department of Physics, Institute of Science and Technology, Erciyes University, Kayseri 38039, Turkey
[b] Department of Physics, Faculty of Arts and Sciences, Erciyes University, Kayseri 38039, Turkey
[c] Department of Physics, Faculty of Arts and Sciences, Nevşehir University, Nevşehir 50300, Turkey

ARTICLE INFO

Article history:
Received 18 August 2010
Received in revised form 28 February 2011
Accepted 10 March 2011
Available online 4 April 2011

Keywords:
Crystal growth
Sn–Sb alloy
Solid–liquid interface energy
Thermal conductivity
Solidification

ABSTRACT

The equilibrated grain boundary groove shapes of solid Sn_3Sb_2 in equilibrium with the Sn–Sb peritectic liquid have been observed from quenched sample with a radial heat flow apparatus. The Gibbs–Thomson coefficient, solid–liquid interfacial energy and grain boundary energy of solid Sn_3Sb_2 have been determined from the observed grain boundary groove shapes. The variation of thermal conductivity with temperature for solid Sn_3Sb_2 and peritectic solid has been measured up to five degree below the meting temperature with a radial heat flow apparatus. The ratio of thermal conductivity of liquid phase to solid phase for Sn–7.8 at.%Sb alloy at the melting temperature has also been measured with a Bridgman type growth apparatus.

1. Introduction

The solid–liquid interfacial energy, σ_{SL}, is recognized to play a key role in a wide range of metallurgical and materials phenomena from wetting [1] and sintering through to phase transformations and coarsening [2]. Thus, a quantitative knowledge of σ_{SL} values is necessary. However, the determination of σ_{SL} is difficult. Since 1985, a technique for the quantification of solid–liquid interfacial free energy from the grain boundary groove shape has been established [3–18]. Observation of groove shape in a thermal gradient can be used to determine the interfacial energy, independent of the grain boundary energy because the interface near the groove must satisfy everywhere.

$$\Delta T_r = \left[\frac{1}{\Delta S_f}\right]\left[\left(\sigma_{SL}+\frac{d^2\sigma_{SL}}{dn_1^2}\right)\kappa_1+\left(\sigma_{SL}+\frac{d^2\sigma_{SL}}{dn_2^2}\right)\kappa_2\right] \quad (1)$$

where ΔT_r, is the curvature undercooling, ΔS_f is the entropy of fusion per unit volume, $n\,(n_x, n_y, n_z)$ is the interface normal, κ_1 and κ_2 are the principal curvatures, and the derivatives are taken along the directions of principal curvature. Thus, the curvature undercooling is a function of curvature, interfacial free energy and the second derivative of the interfacial free energy. Eq. (1) is valid only if the interfacial free energy per unit area is equal to surface tension per unit length, $\sigma_{SL} = \gamma$. When interfacial free energy differs from surface tension, the problem is more complicated and the precise modification of the Gibbs Thomson equation is not yet established [19]. When the solid–liquid interfacial free energy is isotropic, Eq. (1) becomes

$$\Delta T_r = \frac{\sigma_{SL}}{\Delta S_f}\left(\frac{1}{r_1}+\frac{1}{r_2}\right) \quad (2)$$

where r_1 and r_2 are the principal radii of the curvature. For the case of a planar grain boundary intersecting a planar solid–liquid interface, $r_2 = \infty$ and the Eq. (2) becomes

$$\Gamma = r\Delta T_r = \frac{\sigma_{SL}}{\Delta S_f} \quad (3)$$

where Γ is the Gibbs–Thomson coefficient. This equation is called the Gibbs–Thomson relation [13].

At present the most powerful method to measure solid–liquid interface energy experimentally is the grain boundary groove method. This method is based on the direct application of the Gibbs–Thomson equation and can be applied to measure σ_{SL} for multi–component systems as well as pure materials, for opaque materials as well as transparent materials, for any observed grain boundary groove shape and for any value of the thermal conductivity ratio of the equilibrated liquid phase to solid phase, $R = K_L/K_S$.

In general, soldering is performed for the purpose of mechanical or electrical joining. The solder alloys are normally required to be

* Corresponding author. Tel.: +90 352 437 49 01x33114; fax: +90 352 437 49 33.
E-mail address: marasli@erciyes.edu.tr (N. Maraşlı).

0040-6031/$ – see front matter © 2011 Elsevier B.V. All rights reserved.
doi:10.1016/j.tca.2011.03.003

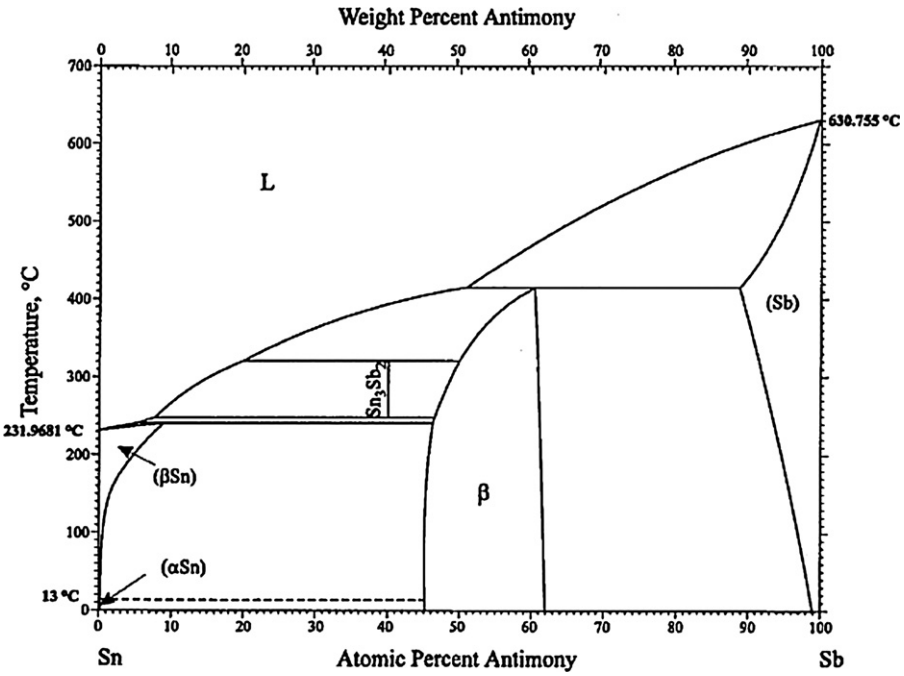

Fig. 1. Phase diagram of Sn–Sb system [20].

superior in joining properties and corrosion resistance. For a long time, the Sn–Pb eutectic has been used as the standard solder for joining electronic components because of its suitable physical and mechanical properties and its low cost. In addition, the solder alloys desirably have high thermal fatigue strength and a desired soldering temperature, and do not contain lead from the environmental point of view. Furthermore, the solder alloys are desirably those which are high in melting point and are not adversely affected by temperature excursions of subsequent processes. Since the tin–lead (Sn–Pb) alloy is low in tensile strength and superior in ductility, it is high in strain generation and low in fatigue strength. Therefore, in conjunction with its low heat resistance, it is low in thermal fatigue strength. The Sn–Sb alloy is relatively higher in strength and is thus better than the (Sn–Pb) alloy. At this time, it is very interesting to study some thermo-physical properties such as solid–liquid interfacial energy, Gibbs–Thomson coefficient, grain boundary energy and thermal conductivity of solid and liquid phases of Sn–Sb alloy. These thermo-physical properties could be of use to people doing comparisons between experimentally observed solidification morphology and predictions from theoretical models. Thus the aim of the present work was to determine the thermal conductivity, Gibbs–Thomson coefficient, solid–liquid interfacial energy and grain boundary energy for solid Sn_3Sb_2 in the Sn–Sb alloy.

2. Experimental

2.1. Sample production

As can be seen from the phase diagram of Sn–Sb alloy as shown in Fig. 1, the peritectic melting temperature is about 518 K and the peritectic liquid composition and the solid solubility of Sb in Sn are Sn–7.8 at.%Sb and Sn–10.3 at.%Sb [20], respectively. Thus, the composition of alloy was chosen to be Sn–16 at.%Sb to grow the solid Sn_3Sb_2 phase on the peritectic structure in a short annealing time. Sn–16 at.%Sb alloy was prepared in a vacuum furnace by using 99.99% pure tin, 99.99% antimony. After stirring, the molten alloy was poured into a graphite crucible held in a specially constructed casting furnace at approximately 50 K above the melting point of alloy. The molten metal was then directionally solidified from bottom to top to ensure that the crucible was completely full. The sample was then placed in the radial heat flow apparatus.

In order to observe the equilibrated grain boundary groove shapes in opaque materials, Gündüz and Hunt [13] designed a radial heat flow apparatus. Maraşlı and Hunt [14] improved the experimental apparatus for higher temperature. The details of the apparatus and experimental procedures are given in Refs. [13–17]. In the present work, a similar apparatus was used to observe the grain boundary groove shapes in the Sn–Sb binary alloy.

As shown in Fig. 2, r_1 is the distance of the controller and measurement thermocouple alumina tubes from the center of the specimen. To place the hot junction of the control thermocouple and one of the measurement thermocouple 0.5–1 mm away from the central alumina tube, the control and the measurement thermocouple holes were drilled at 87° to the ends of the cylinder. The vertical thermocouple and the other measurement thermocouple (r_2) holes were drilled 10–12 mm away from the centre as shown in Fig. 2.

The temperature of the sample was controlled to an accuracy of ±0.01 K with a *Eurotherm 2604* type controller; the temperature of circulating bath was kept constant to an accuracy of ±0.01 K with a *Poly Science Digital 9102* model heating/refrigerating circulating bath. The temperature of the controller was set to 0.1–0.2° above the melting temperature of alloy to get very thin liquid layer around the central alumina tube. Thus, the thickness of the liquid layer around the central alumina tube was controlled by placing the temperature controller thermocouple close to the central alumina tube and setting the annealing temperature 0.1–02° above the melting temperature in the present work.

A thin liquid layer (1–2 mm thick) was melted around the central heating wire and the specimen was annealed in a very stable temperature gradient for a long time. In this condition solid and liquid layers were mixed together. During the annealing period, the liquid droplets move up towards the hot zone of the sample by temperature gradient zone melting and single solid phase can grow. The annealing time for Sn–16 at.%Sb alloy was 4 days. Dur-

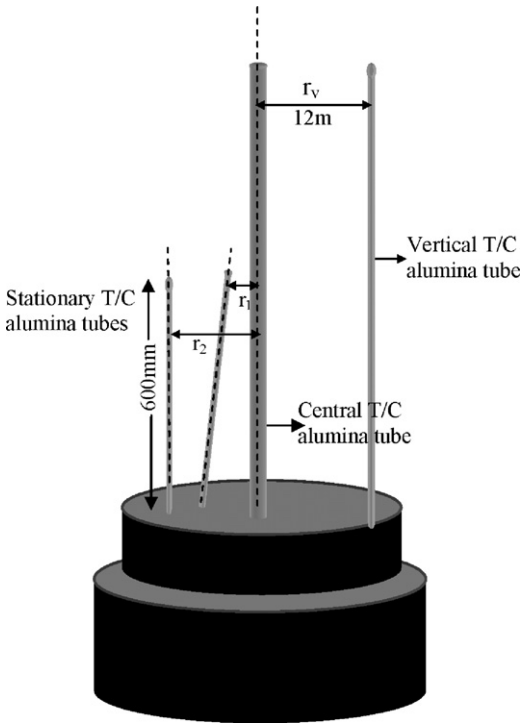

Fig. 2. Longitudinal section view of a part of the sample.

ing the annealing period, the temperature in the specimen and the vertical temperature variations on the sample were continuously recorded by the stationary thermocouples and a moveable thermocouple, respectively by using a data logger via computer. The input power was also recorded periodically. The temperature in the sample was stable to about ±0.025 K for hours and ±0.05 K for up to 4 days. At the end of the annealing time the specimen was rapidly quenched by turning off the input power which was sufficient to get a well defined solid–liquid interface, because the liquid layer around the central heating wire was very thin (typically less than 0.5–1 mm).

2.2. Measurements of the coordinates of equilibrated grain boundary groove shapes

The quenched sample was cut transversely into lengths typically of 25 mm as shown in Fig. 3, and transverse sections were ground flat with 180 grit SiC paper. Grinding and polishing were then carried out by following a standard route. After polishing, the samples were etched with a 10 ml acetic acid and 10 ml nitric acid in 80 ml glycerin for 5 s.

The equilibrated grain boundary groove shapes were then photographed with an Olympus DP12 type CCD digital camera placed on top of an Olympus BX51 type light optical microscope. A graticule ($200 \times 0.01 = 2$ mm) was also photographed using the same objective. The photographs of the equilibrated grain boundary groove shapes and the graticule were superimposed on one another using Adobe PhotoShop 8.0 version software so that accurate measurement of the groove coordinate points on the groove shapes could be made.

2.3. Geometrical correction for the groove coordinates

The coordinates of the cusp, x, y should be measured using the coordinates x, y, z where the x axis is parallel to the solid–liquid interface, the y axis is normal to the solid–liquid interface and the z axis lies at the base of the grain boundary groove. Maraşlı and Hunt [14] devised a geometrical method to make appropriate corrections to the groove shapes and the details of the geometrical method are given in Ref. [14].

The coordinates of equilibrated grain boundary groove shapes were measured with an optical microscope to an accuracy of ±10 μm by following Maraşlı and Hunt's geometrical method so that appropriate corrections to the shape of the grooves could be deduced [14]. The uncertainty in the measurements of equilibrated grain boundary groove coordinates is 0.1%.

2.4. Measurements of the thermal conductivity of solid and liquid phases

The thermal conductivity ratio of equilibrated peritectic liquid phase (Sn–7.8 at.%Sb) to solid Sn_3Sb_2 (Sn–41.4 at.%Sb) phase, $R = (K_{L(\text{peritectic liquid})})/(K_{S(Sn_3Sb_2)})$ must be known or measured to evaluate the Gibbs–Thomson coefficient with the present numerical method. The radial heat flow method is an ideal technique for measuring the thermal conductivity of the solid phase. The thermal conductivity of the solid Sn_3Sb_2 phase is also needed to evaluate the temperature gradient in the solid phases. In the radial heat flow method, a cylindrical sample was heated by using a single heating wire along the axis at the centre of the sample and the sample was kept in a very stable temperature gradient for a period to achieve a steady state condition. At the steady–state condition, the temperature gradient in the cylindrical specimen is given by Fourier's law

$$G_S = \frac{dT}{dr} = -\frac{Q}{2\pi r \ell K_S} \tag{4}$$

where Q is the total input power, r is the distance of the solid–liquid interface to the centre of the sample, ℓ is the length of the heating wire which is constant and K_S is the thermal conductivity of the solid phase. Integration of the Eq. (4) gives

$$K_S = a_0 \frac{Q}{T_1 - T_2} \tag{5}$$

where $a_0 = \ln(r_2/r_1)/2\pi\ell$ is an experimental constant, r_1 and r_2 ($r_2 > r_1$) are fixed distances from the central axis of the specimen, T_1 and T_1 are the temperatures at the fixed positions, r_1 and r_2. Eq. (5) could be used to obtain the thermal conductivity of the solid phase by measuring the difference in temperature between two fixed points for a given power level provided that the vertical temperature variation are minimum or zero.

The thermal conductivities of solid Sn_3Sb_2 (Sn–41.4 at.%Sb) and peritectic solid (Sn–7.8 at.%Sb) phase were measured in the radial heat flow apparatus. Sufficient amount of metallic materials were melted to produce an ingot of approximately 100 mm in length and 30 mm in diameter in a vacuum furnace by using 99.99% pure Sn, 99.99% pure Sb. After stirring, the molten metallic alloy was poured into a graphite crucible held in a specially constructed hot filling furnace at approximately 100 K above the melting temperature of alloy. The molten metallic alloy was then directionally frozen from bottom to top to ensure that the crucible was completely full. The specimen was then placed in the radial heat flow apparatus.

The specimen was heated from the center using a single heating wire (140–190 mm in length and 2.5 mm in diameter, Kanthal A-1) in steps of 50 K up to 10 K below the melting temperature of the material and the outside of the specimen was cooled to maintain a radial temperature gradient. To obtain a reliable value of thermal conductivity in the thermal conductivity measurement, a larger radial temperature gradient is desired. For this purpose, the gap between the cooling jacket and the specimen was filled with free running sand or graphite dust and the outside of the specimen was kept at 293 K using a heating/refrigerating circulating bath. The length of central heating wire was chosen to be 10 mm longer than

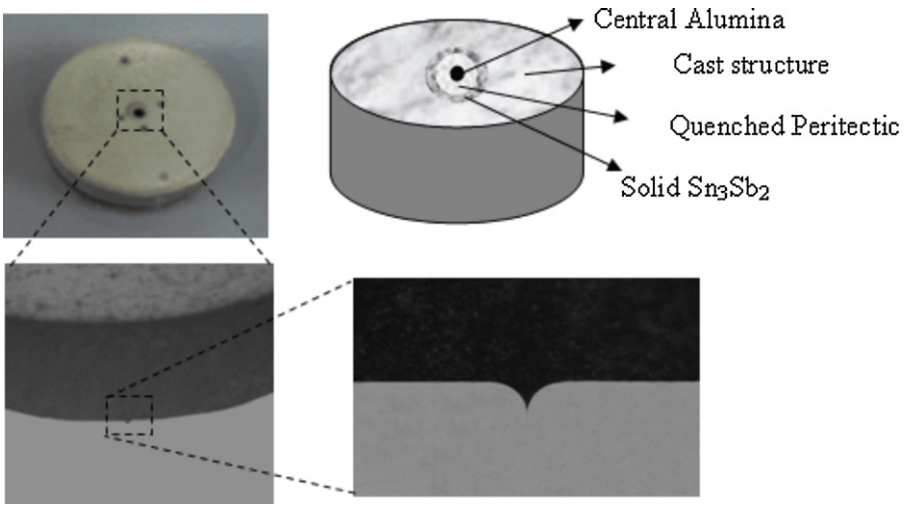

Fig. 3. Illustration of the growth of single solid Sn_3Sb_2 phase from the peritectic liquid on the cast structure.

the length of specimen to make isotherms parallel to the vertical axis.

The specimen was kept at steady state condition for at least 2 h for a setting temperature. At steady state, the total input power and the stationary thermocouple temperatures were recorded with a Hewlett Packard 34401 type multimeter and a Pico TC-08 datalogger. The temperatures on the different parts of the specimen were measured with mineral insulated metal sheathed, 0.5 mm in diameter K type thermocouples. The zero or minimum vertical temperature gradient is desired in thermal conductivity measurements. The vertical temperature for each setting was tried to be made as parallel as possible to the vertical axis by moving the central heater up and down. After all desired power settings and temperature measurements had been completed during the heating procedure, the cooling procedure was started in same steps down to room temperature.

Then the sample was removed from the furnace and cut transversely near to the measurement points, after that the specimen was ground and polished for the measurements of r_1 and r_2. The positions of the thermocouples were then photographed with an Olympus DP12 CCD digital camera placed in conjunction with an Olympus BX51 type light optical microscope. A graticule ($200 \times 0.01 = 2$ mm) was also photographed using the same objective. The photographs of the positions of the thermocouples and the graticule were superimposed on one another using Adobe PhotoShop 8.0 software so that accurate measurement of the distances of stationary thermocouples could be made to an accuracy of ± 10 μm. The transverse and longitudinal sections of the specimen were examined for the porosity, crack and casting defects to make sure that these would not introduce any error to the measurements. The experimental value of a_o for solid Sn_3Sb_2 and peritectic solid (Sn–7.8 at.%Sb) phase were 1.632 m^{-1}, 1.667 m^{-1} in the present work, respectively.

The thermal conductivities of solid Sn_3Sb_2 and peritectic solid phase versus temperature and are shown in Fig. 4. A comparison of thermal conductivities of solid Sn_3Sb_2 and peritectic solid phase with the thermal conductivity of pure Sb [21] and Sn [22] are also given in Fig. 4. The values of K_S for solid Sn_3Sb_2 and peritectic solid (Sn–7.8 at.%Sb) phases at the melting temperature were obtained to be 31.98 W/Km and 40.50 W/Km, respectively by extrapolating to the eutectic temperature as shown in Fig. 4.

A comparison of the thermal conductivity of solid and liquid phases for solid Sn_3Sb_2 and peritectic solid and the thermal conductivity of solid and liquid phases for Sn–5 at.%Sb [23] is given in Table 1.

It is not possible to measure the thermal conductivity of the liquid phase with the radial heat flow apparatus since a thick liquid layer (10 mm) is required. A layer of this size would certainly have led to convection. If the thermal conductivity ratio of the liquid phase to the solid phase is known and the thermal conductivity of the solid phase is measured at the melting temperature, the thermal conductivity of the liquid phase can then be evaluated. The thermal conductivity ratio can be obtained during directional growth with a Bridgman type growth apparatus. The detail of the experimental procedure was given in Refs. [13–17].

The thermal conductivity ratio of the peritectic liquid (Sn–7.8 at.%Sb) to the peritectic solid (Sn–7.8 at.%Sb), $R = (K_{L(\text{peritectic})})/(K_{S(\text{peritectic})})$ was measured to be 0.85 as shown in Fig. 5. The thermal conductivity of peritectic solid phase at the peritectic melting temperature was also measured to be 40.50 W/Km. Thus the thermal conductivity of peritectic liquid phase was determined to be 34.42 W/Km. The value of $R = (K_{L(\text{peritectic})})/(K_{S(Sn_3Sb_2)})$ is also found to be 1.07 by using the values of $K_{L(\text{peritectic})}$ and $K_{S(Sn_3Sb_2)}$. The values of K_L and K_S used in the determination of Gibbs–Thomson coefficient are also given in Table 1.

A comparison of the value of K_S and K_L for Sn–7.8 at.%Sb obtained in the present work with the value of K_S for Sn–5 at.%Sb alloy obtained in the previous work is given in Table 1. As can be seen from Table 1, the value of K_S for Sn–7.8 at.%Sb obtained

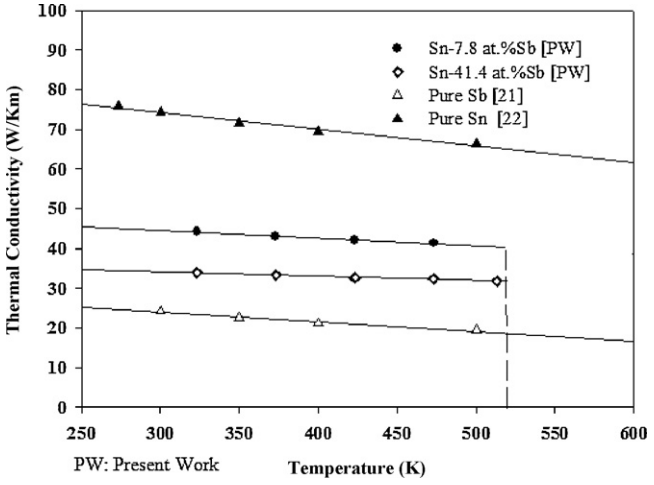

Fig. 4. Thermal conductivity of solid Sn_3Sb_2 and peritectic solid phase versus temperature in the Sn–Sb system.

Table 1
The thermal conductivity of solid and liquid phases and their ratios at their melting temperatures in the Sn–Sb peritectic system.

Alloy	Phases	Melting temperature (K)	K (W/Km)	$R = K_L/K_S$
Sn–Sb	Peritectic liquid (Sn–7.8 at.%Sb)	518.65	34.42	0.85
	Peritectic solid (Sn–7.8 at.%Sb)		40.50	
	Peritectic liquid (Sn–7.8 at.%Sb)	518.65	34.42	1.07
	Solid Sn_3Sb_2 (Sn–41.4 at.%Sb)		31.98	
	Liquid (Sn–5 at.%Sb)	518.65	22 [23]	0.51
	Solid (Sn–5 at.%Sb)		43 [23]	

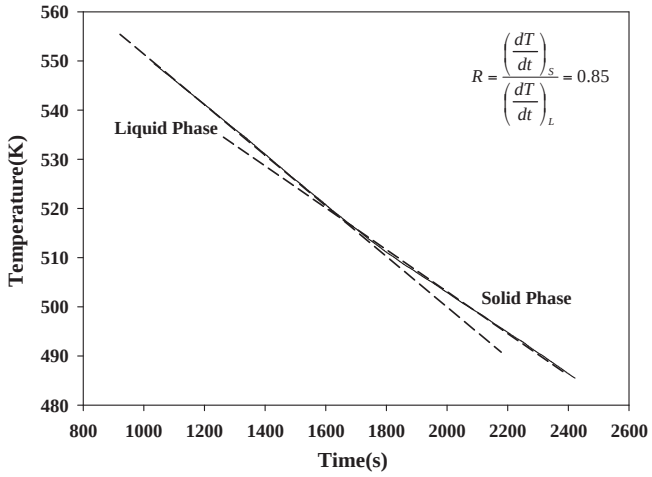

Fig. 5. The cooling rate of Sn–7.8 at.%Sb peritectic alloy.

in the present work agree very well with the value of K_S for Sn–5 at.%Sb alloy obtained in the previous work but the value of K_L for Sn–7.8 at.%Sb obtained in the present work is about 50% bigger than the value of K_S for Sn–5 at.%Sb alloy obtained in the previous work. This difference in the values of K_L might be due to the difference in the composition of liquid phases.

2.5. Measurement of temperature gradient in the solid phase

The average temperature gradient of the solid phase must be determined for each grain boundary groove shape. This was done by measuring the input power, the length of heating wire, the position of the solid–liquid interface and the value of K_S for solid Sn_3Sb_2 phase at the peritectic melting point. By using these measured values in Eq. (4), temperature gradient can be determined for each grain boundary groove shape. The total fractional uncertainty in the measurement of temperature gradient is about 6.5% [14].

3. Results and discussions

3.1. Determination of Gibbs–Thomson coefficient

If the thermal conductivity ratio of equilibrated liquid phase to solid phase, the coordinates of the grain boundary groove shape and the temperature gradient of the solid phase are known, the Gibbs–Thomson coefficient (Γ) can be obtained using the numerical method described in detail in Ref. [13]. The experimental error in the determination of Gibbs–Thomson coefficient is the sum of experimental errors in the measurement of the temperature gradient, thermal conductivity and groove coordinates. Thus the total error in the determination of Gibbs–Thomson coefficient is estimated to be about 7% [14].

The Gibbs–Thomson coefficients for solid Sn_3Sb_2 in equilibrium with the peritectic liquid (Sn–7.8 at.%Sb) were determined with the present numerical model by using ten equilibrated grain boundary groove shapes. Typical grain boundary groove shapes for solid Sn_3Sb_2 in equilibrium with the peritectic liquid (Sn–7.8 at.%Sb) are shown in Fig. 6. The values of Γ for solid Sn_3Sb_2 are given in Table 2. The average value of Γ from Table 2 is $(11.07 \pm 0.8) \times 10^{-8}$ Km for solid Sn_3Sb_2 in equilibrium with the Sn–Sb peritectic liquid.

3.2. Determination of entropy of fusion per unit volume

In order to determine the solid–liquid interfacial energy it is also necessary to know the entropy of fusion per unit volume, ΔS_f for the solid phase. The entropy change per unit volume for an alloy is given by [13],

$$\Delta S_f = \frac{(1 - C_S)(S_A^L - S_A^S) + C_S(S_B^L - S_B^S)}{V_S} \quad (6)$$

where S_A^L, S_A^S, S_B^L and S_B^S are partial molar entropies for A and B materials and C_S is the composition of solid phase. Since the entropy terms are generally not available, for convenience, the undercooling at constant composition may be related to the change in composition at constant temperature. For a solid sphere of radius r [25]

$$\Delta C_r = \frac{2\sigma_{SL} V_S (1 - C_L) C_L}{rRT_M(C_S - C_L)} \quad (7)$$

where R is the gas constant, T_M is the melting temperature and V_S is the molar volume of solid phase. For small changes

$$\Delta T_r = m_L \Delta C_r = \frac{2m_L \sigma_{SL} V_S (1 - C_L) C_L}{rRT_M(C_S - C_L)} \quad (8)$$

where m_L is the slope of liquidus. For spherical solids, the curvature undercooling is

$$\Delta T_r = \frac{2\sigma_{SL}}{r\Delta S_f} \quad (9)$$

From Eqs. (8) and (9), the entropy change for an alloy is written as

$$\Delta S_f = \frac{RT_M}{m_L V_S} \frac{C_S - C_L}{(1 - C_L)C_L} \quad (10)$$

The molar volume, V_S is expressed as

$$V_S = V_c N_a \frac{1}{n} \quad (11)$$

where V_C is the volume of the unit cell, N_a is the Avogadro's number and n is the number of atoms per unit cell. The molar volume of solid Sn_3Sb_2 is 13.87×10^{-5} m^3 [24]. The values of the relevant constant used in the determination of entropy change per unit volume were obtained from phase diagram [20] and are given in Table 3. The error in the determination of entropy change of fusion per unit volume is estimated to be about 5% [26].

3.3. Evaluation of the solid–liquid interfacial energy

If the values of Γ and ΔS_f are known, the value of solid–liquid interfacial energy, σ_{SL} can be evaluated from Eq. (3). The

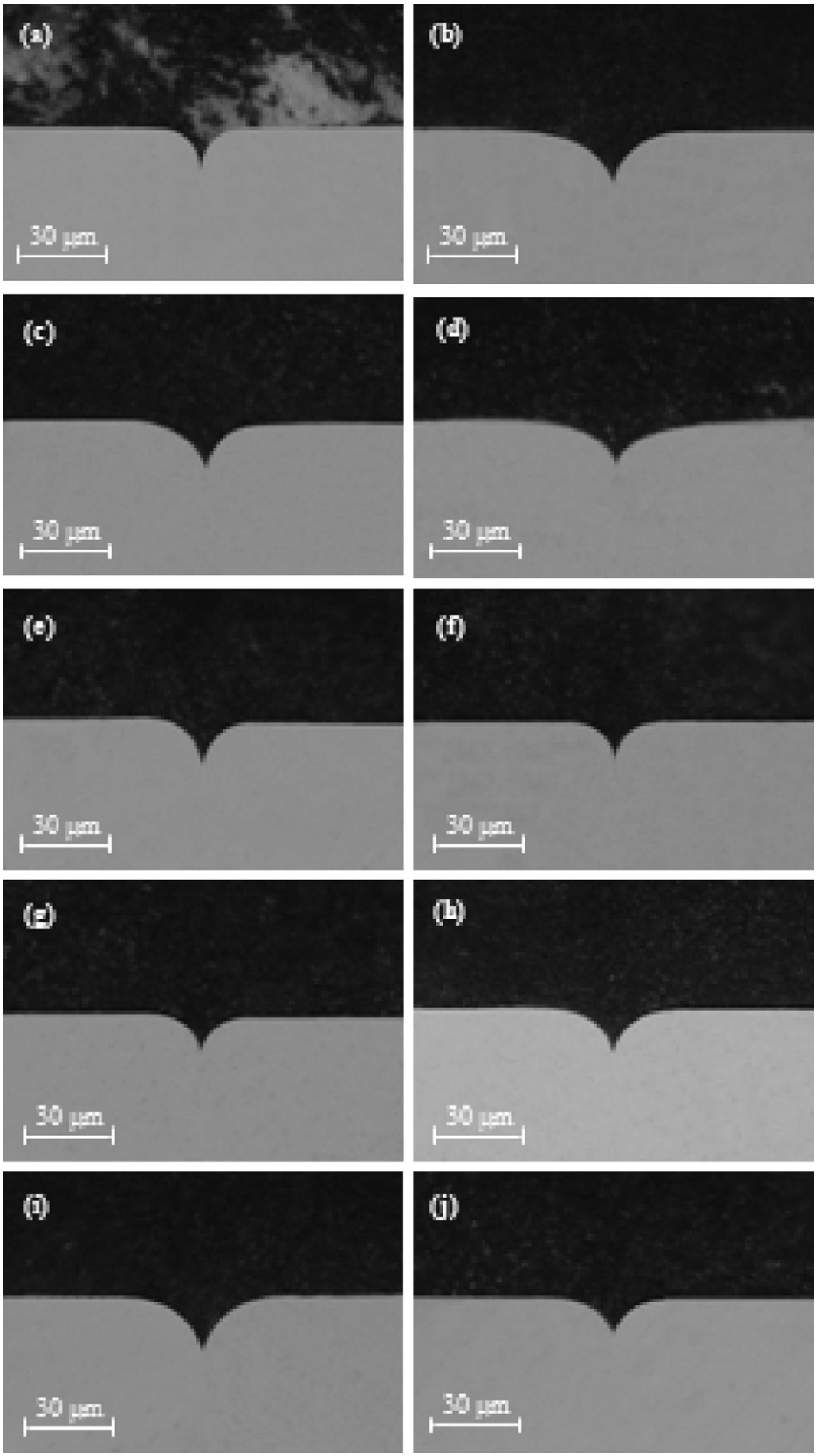

Fig. 6. Typical grain boundary groove shapes for solid Sn_3Sb_2 in equilibrium with the Sn–7.8 at.%Sb peritectic liquid.

Table 2
The Gibbs–Thomson coefficients for solid Sn_3Sb_2 in equilibrium with the Sn–Sb peritectic liquid. The subscripts LHS and RHS refer to left hand side and right hand side of the groove respectively.

Grove no	$G_K \times 10^2$ (K/m)	α^o	β^o	Gibbs–Thomson coefficient	
				$\Gamma_{LHS} \times 10^{-8}$ (K m)	$\Gamma_{RHS} \times 10^{-8}$ (K m)
a	17.26	17.0	14.5	10.56	10.43
b	11.56	14.5	17.6	11.08	11.15
c	11.05	17.8	15.0	11.07	11.17
d	12.46	9.2	9.9	10.88	10.90
e	14.76	7.7	9.2	11.25	11.17
f	18.04	11.5	11.5	11.20	11.13
g	20.16	7.7	9.2	11.17	11.08
h	18.89	14.3	8.5	11.24	11.29
i	12.02	18.4	10.6	11.26	11.24
j	10.08	14.5	14.5	10.98	11.11
				$\bar{\Gamma} = (11.07 \pm 0.8) \times 10^{-8}$ Km	

Table 3
Some thermo-physical properties of solid Sn_3Sb_2 phase in the Sn–Sb peritectic system.

System	Sn–Sb
Composition of solid phase C_S	Solid Sn_3Sb_2 [20] (Sn–41.4 at.%Sb)
Composition of liquid phase C_L	Peritectic liquid [20] (Sn–7.8 at.%Sb)
The value of $f(C)$[a] for solid Sn_3Sb_2	4.73 [20]
Melting temperature, T_m (K)	518.65 [20]
Molar volume of solid Sn_3Sb_2, $V_{Sn3Sb2} \times 10^{-5}$ (m^3)	13.87 [24]
Liquidus slope of solid Sn_3Sb_2, m_L(K/at.fr)	716.86 [20]
Entropy change of fusion for solid Sn_3Sb_2, ΔS_f (J/K m^3)	2.05×10^5

[a] $f(C) = (C_S - C_L)/((1 - C_L)\, C_L)$.

solid–liquid interfacial energy of the solid Sn_3Sb_2 in equilibrium with the peritectic liquid (Sn–7.8 at.%Sb) was evaluated to be $(22.70 \pm 2.7) \times 10^{-3}$ J m^{-2} using the values of Γ and ΔS_f. The experimental error in the determination of solid–liquid interfacial energy is the sum of experimental errors of the Gibbs–Thomson coefficient and the entropy change of fusion per unit volume. Thus, the total experimental error of the solid–liquid interfacial energy evaluation in present work is estimated to be about 12%.

3.4. Grain boundary energy

If the grains on either side of the grain boundary are the same phase then the grain boundary energy can be expressed by

$$\sigma_{gb} = 2\sigma_{SL} \cos \theta \quad (12)$$

where $\theta = (\theta_A + \theta_B)/2$ is the angle that the solid–liquid interfaces make with the y axis. The angles, θ_A and θ_B were obtained from the cusp coordinates, x, y using a Taylor expansion for parts at the base of the groove. According to Eq. (12), the value of σ_{gb} should be smaller or equal to twice of solid–liquid interfacial energy, i.e. $\sigma_{gb} \leq 2\sigma_{SL}$.

The value of the grain boundary energy for the solid Sn_3Sb_2 was found to be $(44.0 \pm 5.7) \times 10^{-3}$ J m^{-2} using the values of the σ_{SL} and θ in Eq. (12). The estimated error in determination of θ angles was found to be 1%. Thus the total experimental error in the resulting grain boundary energy is about 13%.

As mentioned above, interfacial energy anisotropy is considered to play a critical role in many phase transformations. The determination of effects of anisotropy on the interfacial energy is difficult. In literature, there are no theoretical and experimental available data for interfacial energy and also anisotropy of interfacial energy of the solid Sn_3Sb_2 phase.

4. Conclusions

A radial temperature gradient on the sample was established by heating from the center with a single heating wire and cooling the outside of the sample with a heating/refrigerating circulating bath. The equilibrated grain boundary groove shapes for solid Sn_3Sb_2 in the Sn–Sb peritectic alloy were observed from a quenched sample. Some thermo-physical properties such as the Gibbs–Thomson coefficient, solid–liquid interfacial energy and grain boundary energy of solid Sn_3Sb_2 in the Sn–Sb peritectic system have been determined from the observed grain boundary groove shapes. The thermal conductivity of solid Sn_3Sb_2 phase and peritectic solid phase at the peritectic temperature have also been determined.

Acknowledgements

This project was supported by Erciyes University Scientific Research Project Unit under Contract No: FBY–09–679. The authors are grateful to Erciyes University Scientific Research Project Unit for their financial supports.

References

[1] N. Eustathopoulos, M.G. Nicholas, B. Drevet, Wettability at HighTemperatures Pergamon Materials Series, Pergamon, Oxford, 1999.
[2] J.W. Martin, R.D. Doherty, B. Cantor, Stability of Microstructure in Metallic Systems, Cambridge University Press, Cambridge, 1997.
[3] D. Turnbull, J. Appl. Phys. 21 (1950) 1022.
[4] D.R.H. Jones, J. Mater. Sci. 1 (1974) 9.
[5] N. Eustathopoulos, Int. Met. Rev. 28 (1983) 189.
[6] G.F. Bolling, W.A. Tille, J. Appl. Phys. 31 (1960) 1345.
[7] G.E. Nash, M.E. Glicksman, Phila. Mag. 24 (1971) 577.
[8] D.R.H. Jones, G.A. Chadwick, J. Cryst. Growth 11 (1971) 260.
[9] R.J. Schaefer, M.E. Glicksman, J.D. Ayers, Phila. Mag. 32 (1975) 725.
[10] S.C. Hardy, Phila. Mag. 35 (1977) 471.
[11] N.B. Singh, M.E. Glicksman, J. Cryst. Growth 98 (1989) 573.
[12] J.J. Hoyt, M. Asta, T. Haxhimali, A. Karma, R.E. Napolitano, R. Trivedi, MRS Bull. 29 (2004) 935.
[13] M. Gündüz, J.D. Hunt, Acta Mater. 33 (1985) 1651.
[14] N. Maraşlı, J.D. Hunt, Acta Mater. 44 (1996) 1085.
[15] K. Keşlioğlu, N. Maraşlı, Mater. Sci. Eng. A: Struct. Mater. Prop. Microstruct. Process. 369 (2004) 294.
[16] Y. Ocak, S. Akbulut, K. Keşlioğlu, N. Maraşlı, J. Phys. D: Appl. Phys. 41 (2008) 065309.
[17] Y. Ocak, S. Akbulut, K. Keşlioğlu, N. Maraşlı, E. Çadırlı, H. Kaya, Experimental determination of interfacial energies for Ag_2Al solid solution in the $CuAl_2$-Ag_2Al syste, Chinese Physics B 18 (9) (2009) 3952–3959.
[18] A. Bulla, C. Carreno, B. Bodensiek, R. Pustal, Berger, A. Bührig, A. Polaczek, Ludwig. Metall. Mater. Trans. A 38 (2007) 1956.
[19] R. Trivedi, J.D. Hunt, The Mechanics of Solder Alloy Wetting and Spreading, Van Nostrand Reinhold, New York, 1993, p. 191.
[20] M. Hansen, K. Anderko, Constitutions of Binary Alloys, McGraw-Hill Book Company, New York, 1958, p. 1175.

[21] Y.S. Touloukian, R.W. Powell, C.Y. Ho, P.G. Klemens, Thermal Conductivity Metallic Elements and Alloys. The TPRC Data Series, vol. 1, IFI/Plenum, New York, Washington, 1970, pp. 10–14.
[22] Y.S. Touloukian, R.W. Powell, C.Y. Ho, P.G. Klemens, Thermal Conductivity Metallic Elements and Alloys. The TPRC Data Series, vol. 1, IFI/Plenum, New York, Washington, 1970, pp. 389–408.
[23] S. Mhiaoui, F. Sar, J.G. Gasser, J. Non-Cryst. Solids 353 (2007) 3628.
[24] N. Navida, G. Andriy, R. Peter, S. Adriana, G. Gerald, J. Solid State Chem. 182 (2009) 645–656.
[25] J.W. Christian, The Theory of Transformations in Metals and Alloys Part I, 2nd edn., Pergamon, Oxford, 1975, 169.
[26] M. Tassa, J.D. Hunt, J. Cryst. Growth 34 (1976) 38.